**Acta Acustica united with Acustica**
**Vol. 95 (2009) 46 – 59**

DOI 10.3813/AAA.918126

# Efficiency of Energy Conversion in Underwater Spark Discharges and Associated Bubble Oscillations: Experimental Results

Silvano Buogo
CNR – Istituto di Acustica "O. M. Corbino", via Fosso del Cavaliere 100, 00133 Roma, Italy.
silvano.buogo@idac.rm.cnr.it

Jaroslav Plocek
Physics Department, Faculty of Electrical Engineering, Czech Technical University in Prague, Technická 2, 166 00 Praha 6, Czech Republic. plocek@fel.cvut.cz

Karel Vokurka
Physics Department, Technical University of Liberec, Hálkova 6, 461 17 Liberec, Czech Republic.
karel.vokurka@tul.cz

**Summary**
In this paper low-voltage high-energy spark discharges in water and associated bubble oscillations are studied experimentally. Pressure waves emitted during spark discharges and during following bubble oscillations have been recorded and analyzed to determine the radiated acoustic energy and potential energy of the bubbles. These energies are then used to determine the efficiency of energy conversion. For example, it has been found out that only 2% to 8% of electrical energy stored in the capacitor bank is converted into the potential energy of the bubble at its first maximum volume and only about 30% of this potential energy is radiated as acoustic energy in the first bubble pulse. Due to specific features of the low-voltage apparatus used, bubbles of different sizes have been generated and these bubbles were found to oscillate with different intensities. To explain this great diversity in the generated bubbles, the electrical circuit of the apparatus and the early stages of the spark discharge are analyzed. While it is confirmed that the bubble size grows with the energy used for discharge, the relation between the intensity of bubble oscillations and the circuit parameters is more complex. To explain this relation, two hypotheses, partly supported by the data available, are presented. The first hypothesis concerns the rate of electrical energy delivery into the discharge channel, and the second hypothesis concerns the efficiency of electrical energy conversion into heat in the discharge channel.

**PACS no. 43.30.Jx, 43.30.Lz**

## 1. Introduction

Underwater spark discharges have been exploited in many diverse applications. For example, they have been used as impulsive sound sources for deep-sea prospecting [1, 2], for minesweeping applications [3], as shock wave sources in medicine [4, 5, 6], and as convenient means to study bubble dynamics [7, 8, 9]. Despite many successful applications and great efforts devoted to understanding this physical phenomenon [1, 2, 10, 11, 12, 13, 14, 15, 16, 17, 18, 19, 20, 21, 22], not all details have been satisfactorily clarified yet. The reason can be seen in the relative complexity of this fast evolving dynamic nonlinear phenomenon, which, to a certain degree, has also a random character.

Received 1 February 2007,
accepted 17 November 2008.

The phenomenon considered can be divided into two processes: (1) an initial spark discharge, and (2) a subsequent bubble formation and oscillation. The spark discharge is initiated by connecting a capacitor charged to a sufficiently high voltage to two electrodes submerged in a liquid. The high intensity electric field between the two electrodes causes a breakdown of the liquid and formation of a conducting plasma channel. Due to the flow of a large electric current pulse through the channel, the plasma is violently heated, and the channel explosively expands and converts into an oscillating bubble. These two processes, the initial spark discharge and subsequent bubble oscillations, are tightly interconnected and it may be of interest to know how the parameters of the spark discharge determine the properties of the oscillating bubble.

The intensity and time evolution of the spark discharge are determined by the charging voltage $V$, the capacitance $C$, the circuit inductance $L$ and resistance $R$, the discharge

electrodes configuration, the working liquid properties, and the hydrostatic pressure in the liquid. The mutual relation of these parameters determines the total energy $E_c$ available for the discharge and the portion of this energy $E_d$ delivered into the channel, the liquid breakdown time $t_b$, and the frequency and damping of the oscillatory discharge current $i(t)$ and associated voltage $v(t)$. The electrode configuration also has a fundamental influence on the repeatability of the successive discharges. Even if descriptions of some real discharge circuits and the forms of the discharge currents and voltages can be found in the literature (see, e.g., references [14, 17, 22]), a unifying theory encompassing the influence of different values of $V$, $C$, $L$, $R$, etc. is still missing. Thus the design of new circuits is largely based on trial and error.

Regarding the bubble generated by the discharge, it can be described using its maximum size and intensity of oscillation [23]. It can be expected that, to a certain degree, the bubble size will be directly proportional to the energy delivered into the channel [22]. However, no information can be found in the literature concerning the factors influencing the intensity of bubble oscillation.

Most experimental work described in literature [10, 11, 14, 15, 16, 22] has concentrated on studying peak pressures of pulses originating during the initial explosive channel growth and on the time of the first bubble oscillation. Only very limited attention [15, 16] has been paid to the acoustic energy carried away by the radiated pressure waves and to further bubble oscillations.

In this paper several of the questions mentioned above shall be addressed. The analysis presented here is based on a large set of experimentally determined pressure wave records measured with a broadband hydrophone. Firstly, the electrical parameters of the discharge circuit and the early stages of the discharge will be analyzed with the aim of obtaining a better understanding of the generated bubble properties. Then the efficiency will be determined with which the energy $E_c$ available for the spark discharge is converted into acoustic and potential energy of the bubble. Finally it will be analyzed how the discharge circuit parameters $C$ and $R$ influence the intensity of bubble oscillations. Results discussed here have been presented in a shortened form at a conference [24].

## 2. Experimental setup

Figure 1 shows the experimental setup used to study the underwater spark discharges and associated oscillating bubbles. The spark discharges were produced using as a sparker two electrodes made of tungsten wire with diameter 1.3 mm and length between 30 mm and 50 mm, mounted on conical holders made of brass with the electrode tips facing each other with a gap length variable up to about 2 mm, and with their axes in an horizontal plane and making an angle between about 120 degrees and 180 degrees, depending on the measurement session. The electrodes were connected via a 5 m cable to a capacitor bank consisting of 9 capacitors, each with capacitance 40 µF. By connecting these capacitors in parallel,

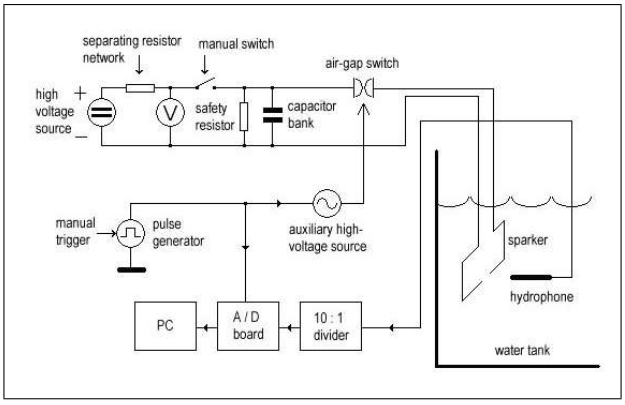


Figure 1. Experimental setup used for studying acoustic emission from spark discharges and generated bubbles.

the total capacitance could be varied in 40 µF steps from 40 µF to 360 µF. The capacitors were charged from a high voltage source to voltages ranging from 2.0 kV to 2.6 kV, with most experiments done using voltages near 2.5 kV. Due to the relatively low value of the high voltage source employed, the discharges are referred to as being "low-voltage" discharges, as discharges done with higher voltages may differ substantially. A manual switch was used to initiate charging of the capacitors; for safety reasons the charging was switched off after each experiment. A digital voltmeter was used to measure the charging voltage. Series resistors and shunt resistors were included in the circuit for safety reasons. Due to their high values these resistors play no role in the discharge process. The capacitor bank was connected to the sparker through an auxiliary air-gap switch, which was triggered manually by a pulse generator. The manual trigger pulse also started data acquisition of the A/D board. The sparker was submerged in a laboratory water tank 6 m long, 4 m wide and 5.5 m deep, filled with fresh water at room temperature. The electrodes were positioned at 2.75 m depth and approximately 1.5 m away from the nearest tank wall. Due to the high electrical energies employed, the generated bubbles were of relatively large size ranging from about 30 mm to 110 mm in diameter.

The apparatus used in the present experiments (the capacitor bank, the high-voltage source, and the sparker) was originally designed for high resolution sea prospecting [1, 2] and for our experiments it was modified to minimize the interaction of the electrodes with the generated bubbles and the acoustic reflections from the holders and supporting elements. However, using thinner electrodes had a consequence that the electrodes burnt away rather quickly, with the gap length $d$ increasing from one discharge to another, thus causing large differences between subsequent discharges. As a result, the repeatability of the discharges and associated phenomena was poor. However, as an unexpected side-effect it was possible to generate bubbles oscillating with a wide range of intensities.

Pressure waves radiated by the explosively growing channel and by the resulting oscillating bubble were recorded using a broadband hydrophone (Reson, type

TC 4034) with low-frequency receiving sensitivity of −216.5 dB re 1 V/μPa. The hydrophone's usable frequency range extends from 1 Hz to 470 kHz with variations in sensitivity within (+2 dB, −10 dB) with respect to the low-frequency value, reducing to (+2 dB, −4 dB) for frequencies up to 410 kHz. The hydrophone was positioned at the same depth as the discharge electrodes with its main axis pointing towards the sparker gap. Three distances $r$ of the hydrophone acoustic center from the center of the sparker gap have been used in the experiments: 0.5 m, 0.25 m, and 0.1 m. The shortest distance gave the best signals with lowest level of reflections. However, because of very high transient pressures measured, of the order of several MPa, the risk of hydrophone damage was the highest in this case and for this reason only a limited number of records were taken at this distance.

As the hydrophone output voltage often exceeded the maximum A/D board input range, a 10:1 voltage divider was inserted between the hydrophone and the A/D board. The divider's frequency response was flat from DC to 1 MHz and its input impedance was 1 MΩ. The low impedance output of the divider was connected to the input of the A/D board (National Instruments, type PCI 6115) having 12 bit resolution and 10 MHz sampling rate. Each acquired record consisted of $2 \times 10^5$ samples, corresponding to a record length of 20 ms. The acquired digital records have been transferred to and stored into a personal computer for further processing.

The experiments were done in series made of several individual discharges. At the beginning of each series the gap length $d$ between the electrodes was set to approximately 0.1 mm. After each discharge a small amount of the electrodes melted down and thus the gap increased slightly. When, after several discharges, the gap broadened to about 2 mm, no more discharges occurred with the available voltage. Hence the sparker had to be taken out of the water, the gap set to the initial value of $d \approx 0.1$ mm and a new series of discharges could begin. The number of discharges in different series varied from 2 to about 15, with more discharges in one series for small discharge energies $E_c$, and less discharges for large energies $E_c$. An interesting feature was that the lower energy discharges terminated for a shorter gap length than the higher energy discharges.

As said before, one of the earliest findings after all data were collected and processed was the wide range of oscillation intensities, to which the generated bubbles have been excited. A similar phenomenon has not been described elsewhere in the literature. By careful data analysis we have noticed that the intensity of bubble oscillations was rather low at the beginning of each series and higher at the end of it, increasing with the position of an individual discharge in each series. It is important to note that even if these changes in oscillation intensity can be seen by an experienced observer already in the raw data, they are often not recognized at first sight since there are usually many other parameter changes involved (e.g., capacitance $C$, charging voltage $V$, bubble size, etc.).

The wide range of bubble oscillation intensities is a valuable result that will be discussed in a next paper on bubble dynamics. However, the cause for such a large scatter requires at first to look for an explanation. Some results of this endeavor are given in section 7. However, it has been also found out that to explain all trends and peculiarities in the data observed, a much larger set of experimental data than the present one would be necessary.

Even if the gap length is certainly an important parameter for the processes studied, it was not measured directly for two reasons. First, due to the irregular surfaces of the burnt electrodes tips this would hardly give an accurate result. Second, with this experimental setup measuring the gap length would require removing the sparker from water after each discharge, which would slow down data collecting considerably. Indeed, the importance of the gap length for the present analysis became evident only after the experiments were done during the analysis of collected data.

Nevertheless, a possible indicator of the gap length was found to be the position of the discharge in a series. However, because of different lengths of the series and because the gap length is increasing faster at the end of each series than at the beginning, the ordinary numbering of discharges in the series has shown to be of little use. Instead of that a reversed order of discharge numbering has proved to be helpful. Therefore the discharges within each series have been renumbered in a reversed order, i.e. number one ($n = 1$) was assigned to the last successful discharge in the series, number two ($n = 2$) to the second discharge from the end, and so on. In section 7 this numbering will be interpreted as an indicator of the gap length $d$ and thus also as an indicator of the discharge channel resistance $R_d$. It should be stressed here that this approach serves here only as an auxiliary means for basic interpretation of data, and in no case it can be a substitute for the real measurement of the discharge channel resistance $R_d$. The experimental determination of $R_d$, even if it is not a trivial task, seems at present as the only possible way to have a deeper insight into the processes studied and should accompany any future research in this area.

To check the shape and the overall behavior of the generated bubbles, a limited number of oscillating bubbles were also recorded using a high-speed camera (Photec 16-mm film full-frame rotating prism camera), with frame rate set to about 3000 frames per second. The camera was positioned behind a glass window in a chamber adjacent to the water tank, while the volume where the oscillating bubble originated was illuminated continuously using a submerged inclined mirror and two lamps clamped above the water surface. With each film record a corresponding pressure wave record was also acquired. After the films were developed, up to 100 selected frames, for a total record length of about 33 ms, were digitized for further analysis.

## 3. Analysis of the discharge circuit

In this section an analysis of the discharge circuit is presented. The circuit is basically a series connection of a capacitor with capacitance $C$, and of cables, air-gap switch

and sparker having overall inductance $L$, and resistance $R$. Of these, only the capacitor can be considered to be a lumped element. The inductance and resistance are distributed elements in any case. Furthermore, as it will be pointed out later on, a part of the resistance of the discharge circuit is not constant.

A few basic equations of circuit theory are recalled here for convenience, since they will be exploited in the following discussion. The capacitance $C$ and the charging voltage $V$ determine the overall energy available for the spark discharge,

$$E_c = \frac{1}{2} C V^2. \tag{1}$$

The current $i(t)$ flowing through the discharge circuit can be determined theoretically from the differential equation

$$\frac{\mathrm{d}^2 i}{\mathrm{d}t^2} + \frac{R}{L}\frac{\mathrm{d}i}{\mathrm{d}t} + \frac{1}{LC} i = 0. \tag{2}$$

The discharge current $i(t)$ has an oscillatory character and depending on the mutual relation of $C$, $L$ and $R$, it can be in the form of damped, critically damped, and overdamped oscillations. As will be shown later, only damped oscillations have been generated in the experiments studied here. In this case the theoretical form of the current is given by

$$i(t) = -\frac{V}{\omega_d L} \mathrm{e}^{\beta t} \sin\left(\omega_d t\right). \tag{3}$$

Similarly, the voltage across the capacitor $v_C(t)$ can be expressed in the form

$$v_C(t) = -\frac{V}{\omega_d} \mathrm{e}^{\beta t} \left[\beta \sin\left(\omega_d t\right) - \omega_d \cos\left(\omega_d t\right)\right]. \tag{4}$$

In these equations $\beta = -R/(2L)$ is a damping constant and $\omega_d$ is a natural angular frequency of damped oscillations ($\omega_d^2 = \omega_n^2 - \beta^2$). Finally $\omega_n = 1/\sqrt{LC}$ is a natural angular frequency of un-damped oscillations.

When analyzing the sparker performance, the maximum value of $i(t)$ and the rate of growth of $i(t)$ are of interest. As can be seen from equation (3), these values depend on the inductance $L$, angular frequency $\omega_d$ and damping constant $\beta$. And the values of $\omega_d$ and $\beta$ are determined by the mutual relation of $C$, $L$ and $R$.

The capacitance $C$ is determined directly from the characteristics of the capacitor employed, and if need is to check its nominal value, this can be done easily, for instance, with an RLC meter. The remaining two parameters, $R$ and $L$, are more involved and deserve a brief discussion.

The resistance of the discharge circuit $R$ enters into the relation for the damping constant $\beta$, and thus determines also the time constants. The resistance $R$ consists of several parts

$$R = R_i + R_c + R_a + R_d. \tag{5}$$

Here $R_i$ is the inner resistance of the capacitor, $R_c$ is the resistance of the connecting cables, $R_a$ is the resistance of the air-gap switch, and $R_d$ is the resistance of the discharge channel. Whereas the inner resistance $R_i$ and the resistance of the cables $R_c$ are constant, the remaining two resistances ($R_a$ and $R_d$) vary with the current $i(t)$, are thus time dependent and may attain different values in different discharges, partially in a random manner [12]. The relation between the resistances determines the efficiency $\eta_d$ with which the energy $E_c$ is converted into Joule heat in the discharge channel $E_d$,

$$\eta_d = \frac{R_{d\,\mathrm{ef}}}{R_{\mathrm{ef}}} = \frac{E_d}{E_c}, \tag{6}$$

assuming that the available energy at breakdown, $E_b$, is equal to energy $E_c$ (actually, this is not true, as usually $E_b < E_c$ due to the pre-breakdown current). The resistances $R_{d\,\mathrm{ef}}$ and $R_{\mathrm{ef}}$ represent certain mean (effective) values of $R_d(t)$ and $R(t)$, respectively, which fulfill the validity of equation (6).

Relation (6) is of primary interest in the analysis of sparker performance and in evaluating experimental data. However, only one part of the resistance $R$, namely the resistance $R_c$, can be determined easily. The resistance of the connecting cables has been measured in the present case using an RLC meter and it was found to be $R_c = 0.04\,\Omega$. The resistance of the discharge channel $R_d$ is influenced by the channel length, by the cross section area of the channel and by the degree of ionization of the vapor in the channel. While the channel length is determined by the gap $d$ between the electrodes first of all, not much can be said at present about the channel cross-section area and the degree of vapor ionization. And due to specific behavior of the discharge channel, the resistance $R_d$ varies with the current $i(t)$, that is, the resistance $R_d$ is nonlinear and is also time dependent.

The inductance $L$ consists of several parts again, the most important being the internal inductance of the capacitor and the inductance of the connecting cables. The inductance $L$ influences both the damping constant $\beta$ and the natural angular frequency $\omega_n$. Theoretical analysis and computations show that low values of $L$ are necessary for obtaining high values of $i(t)$, and high rates of growth of $i(t)$. Using the RLC meter the inductance of the connecting cables (without the cables to the air-gap switch) was measured to be $L = 6.3\,\mu\mathrm{H}$.

All the electrical parameters mentioned so far will influence the instantaneous power

$$P_d(t) = R_d(t)\, i^2(t), \tag{7}$$

and the energy delivered into the discharge channel up to the time $t$,

$$E_d(t) = \int_{t_b}^{t} P_d(\xi)\, \mathrm{d}\xi. \tag{8}$$

During the present experiments the time-varying current $i(t)$ and voltage $v(t)$ were not measured. However, to obtain a better understanding of the discharge circuit, a few additional tests were done at a later time after completing

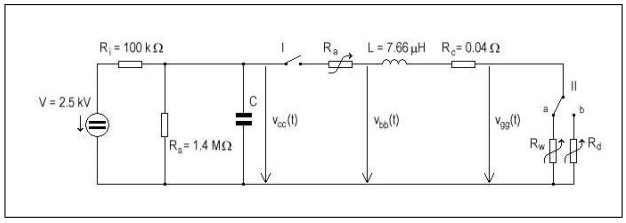


Figure 2. An equivalent scheme of the discharge circuit.

the basic experiments. In these tests a high voltage probe (Tektronix type A6302) was connected first to the capacitor terminals, then to the cables after the air-gap switch and finally just across the discharge gap (voltages $v_{cc}(t)$, $v_{bb}(t)$ and $v_{gg}(t)$, respectively, see Figure 2). The time evolutions of these voltages have been recorded using a digitizing oscilloscope (Tektronix TDS420). Altogether 36 records have been obtained corresponding to different capacitances and different gaps between the electrodes. By analyzing these records an equivalent scheme of the discharge circuit could be determined. This scheme is given in Figure 2.

In the equivalent scheme the switch I substitutes the air-gap switch. Voltage records revealed that this switch does not close immediately after sending the trigger pulse, but after a certain delay $t_a$. This delay varies from one experiment to another in a random manner. In the present limited series of 36 experiments, the values of $t_a$ ranged from 130 μs to 1200 μs with a mean value of 236 μs. The resistor $R_a$ represents the resistance of the air-gap switch.

After switch I is closed, a pre-breakdown interval starts. During this interval switch II is in position $a$, and the capacitor is discharged through the resistor $R_w$. The analysis of voltage records showed that the duration of the pre-breakdown interval $t_b$ is closely related to the gap length $d$. For touching tungsten electrodes ($d \approx 0$ mm) the pre-breakdown interval length was also $t_b \approx 0$ s. On the other hand, if no breakdown occurred due to an excessive gap length ($d > 2$ mm), the pre-breakdown interval length was $t_b \to \infty$. For example, the values of $t_b$ within one series of experiments were successively 2, 18, 78, 628, and 1204 μs. In this example the initial gap was about $d \approx 0.1$ mm and the final gap was about $d \approx 2$ mm. The capacitance was 280 μF. By analyzing the voltage records it was determined that in different experiments the mean value of the resistance $R_w$ ranged from about 20 Ω to 40 Ω. Thus the mean value of the current $i(t)$ in the pre-breakdown interval also ranged from about 60 A to about 120 A.

When breakdown occurs, switch II toggles to position $b$, and the current $i(t)$ starts flowing through the resistor $R_d$. This resistor represents the resistance of the discharge channel and its value is approximately 200 times lower than the resistance of $R_w$. The resistors $R_a$, and $R_d$ are nonlinear (their values vary with the current), time-varying, and in different experiments they take on different values in a random manner.

As mentioned above, the capacitance $C$ and the inductance $L$ and resistance $R_c$ of the connecting cables have

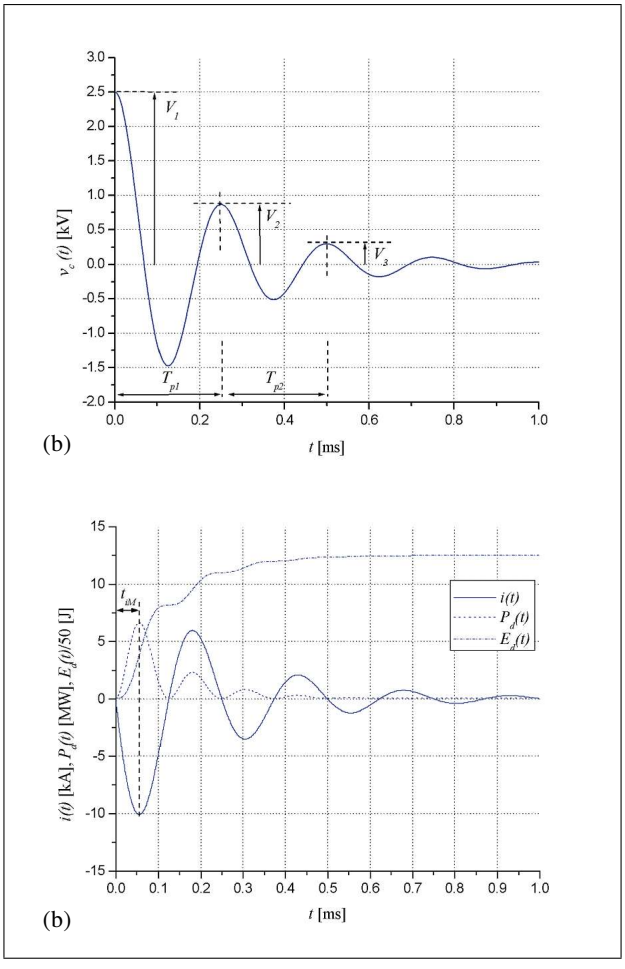


Figure 3. a. Variation of voltage $v_C(t)$ with time. $C = 200$ μF, $L = 7.66$ μH, $R = 0.065$ Ω. $V_1$, $V_2$, $V_3$ are voltage amplitudes in periods $T_{p1}$ and $T_{p2}$. b. Calculated time dependences of the discharge current $i(t)$ (solid curve), instantaneous power $P_d(t)$ (dashed curve) and energy $E_d$(t) (dash-dot curve) for $C = 200$ μF, $L = 7.66$ μH and $R = 0.065$ Ω.

been measured using an RLC meter. During the measurements of $L$ and $R_c$ the sparker gap was short-circuited. To obtain an estimate of the resistances of the air-gap switch $R_a$ and of the discharge channel $R_d$, a code based on equations (3)–(4) and (7)–(8) was written in MATLAB. In this way theoretical time dependences of the current $i(t)$, voltage $v_C(t)$, power $P_d(t)$, and energy $E_d(t)$ could be computed for different values of $C$, $L$ and $R$ (in these computations it was assumed that the overall circuit resistance $R$ is constant). An example of the computed voltage $v_C(t)$ is given in Figure 3a.

For each experimental record voltages $v_{cc}(t)$ and $v_{bb}(t)$, the damping ratio $V_{n+1}/V_n$ and the periods of oscillation $T_{pn}$, $n = 1$, 2, and 3 were determined (for a definition of these quantities see Figure 3a). Using the MATLAB code and varying the values of $C$, $L$ and $R$ it was possible to determine the best fit of the computed voltages $v_C(t)$ to the experimentally determined damping ratios and periods of oscillations. The total circuit inductance, including the inductance of connecting cables, air-gap switch, sparker, and

the internal inductance of the capacitor, was found to be $L = 7.66\,\mu\text{H}$. However, it is remarked that the values of $L$ determined for different discharges were slightly different, and the value of $L$ given above is an ensemble average.

As already mentioned, in a real discharge circuit the resistors $R_a(t)$ and $R_d(t)$ are time-varying. Hence the value of the resistor $R$ determined by comparing the theoretical and experimental damping ratios and periods of oscillations can be interpreted as a time average value $R_{\text{mean}}$. And as given in equation (5), this time average resistance is composed of four parts, namely of $R_c$, $R_i$, $R_{a\,\text{mean}}$ and $R_{d\,\text{mean}}$. Computation of $R_{\text{mean}}$ has been done for each record $v_{cc}(t)$ and $v_{bb}(t)$ and for each period of oscillations separately. For the first period of oscillation it was found that $R_{\text{mean1}} = 0.065 \pm 0.008\,\Omega$ and for the second period $R_{\text{mean2}} = 0.088 \pm 0.009\,\Omega$. These values are ensemble averages again, calculated from 14 and 10 time averages, respectively. After neglecting $R_i$ and subtracting the value of $R_c = 0.04\,\Omega$ from $R_{\text{mean1}}$ and $R_{\text{mean2}}$ one obtains that $R_{\text{mean1}} + R_{\text{mean1}} \approx 0.025\,\Omega$ and $R_{a\,\text{mean2}} + R_{d\,\text{mean2}} \approx 0.045\,\Omega$. Assuming further that $R_{a\,\text{mean1}} \approx R_{a\,\text{mean2}} \approx R_{d\,\text{mean1}}$ one obtains that $R_{d\,\text{mean1}} \approx 0.0125\,\Omega$ and $R_{d\,\text{mean2}} \approx 0.0325\,\Omega$.

An example of the computed current $i(t)$, instantaneous power $P_d(t)$, and energy $E_d(t)$ is shown in Figure 3b. In Figure 3b the time $t_{iM}$ denotes the instant when the current $i(t)$ (and thus also the power $P_d(t)$ dissipated in the resistor $R$) attains its first maximum value. As will be shown later, the values of $t_{iM}$ may play a certain role in influencing the intensity of oscillations of the generated bubbles. Therefore, using the values of $L$ and $R$ determined above and the values of the capacitance $C$ used in these experiments, theoretical values of $t_{iM}$ have also been computed. These results will be used later in section 5 (Figure 7) and in section 7.

## 4. Experimental records

When the capacitor charged to voltage $V$ is connected to the submerged electrodes, breakdown of the liquid occurs after a time $t_b$. After breakdown, a certain part of the energy $E_c$ stored in the capacitor is delivered into the discharge channel and heats the plasma. This delivered energy has been denoted as $E_d$.

As a consequence of Joule heating of the plasma, pressure and temperature in the channel start increasing violently. Due to the high pressure the discharge channel grows explosively and converts into a radially oscillating (pulsating) bubble. This bubble first grows to a maximum volume. After reaching its maximum volume at a time $t_1$, it attains its maximum potential energy $E_{\text{pot1}}$. At this time the bubble wall motion reverts and the bubble enters a compression phase, during which it reaches a minimum volume at a time $t_{p1}$. At the minimum volume the bubble wall motion reverts again and the bubble expands to a second maximum volume, which it reaches at a time $t_2$. Next, a new compression phase starts, a second minimum volume is attained at a time $t_{p2}$, a new expansion phase follows, and so on.

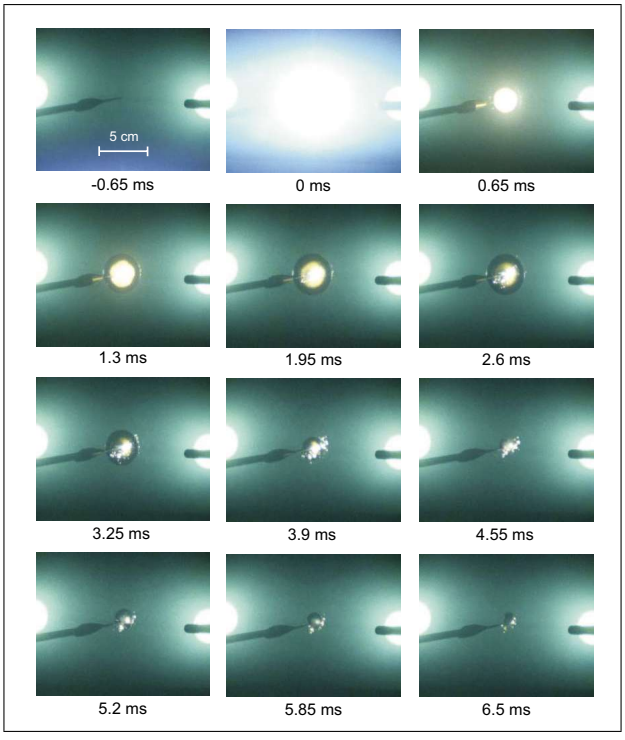


Figure 4. Selected frames from a typical film record. The time in ms elapsed after breakdown is shown under each frame.

The bubble wall motion is accompanied by emission of pressure waves into the surrounding liquid: an oscillating (pulsating) bubble is an excellent zero-order acoustic radiator. The positive peak pressures are radiated when the bubble attains minimum volumes at times $t_{p1}, t_{p2}, \ldots$, and the maxima of negative pressure, that in the following discussion will be referred to as trough pressures, are radiated at maximum bubble volumes at times $t_1, t_2, \ldots$. (As all the time data are derived from the pressure records in this work, for simplicity the same notation has been used for the bubble wall motion events and for the pressure waves received at a distance $r$ from the bubble center, though the pressure data are retarded with respect to the bubble wall data by a propagation time $\Delta t = r/c_\infty$, where $c_\infty$ is the speed of sound in the liquid). The radiated pressure wave carries away from the bubble a part of the delivered energy $E_d$ in form of acoustic energy $E_a$.

Altogether 10 films have been taken in experiments, where both bubble oscillations and radiated pressure waves have been recorded. A few selected frames from one of the film records are shown in Figure 4. From the film records it was verified that the generated bubbles possess an almost spherical shape during prevailing portions of their lifetime, especially close to maximum volumes, and they retain spherical shape in these portions at least during the first two oscillations. Certainly due to low framing rate of the high speed camera and due to the film overexposure by light emitted when the bubble is near its minimum volume nothing can be said about the bubble shape

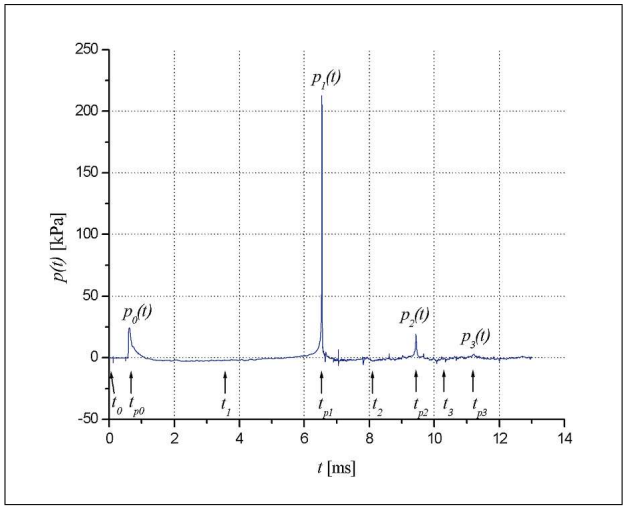


Figure 5. An example of the pressure wave $p(t)$ normalized to a distance $r = 1$ m.

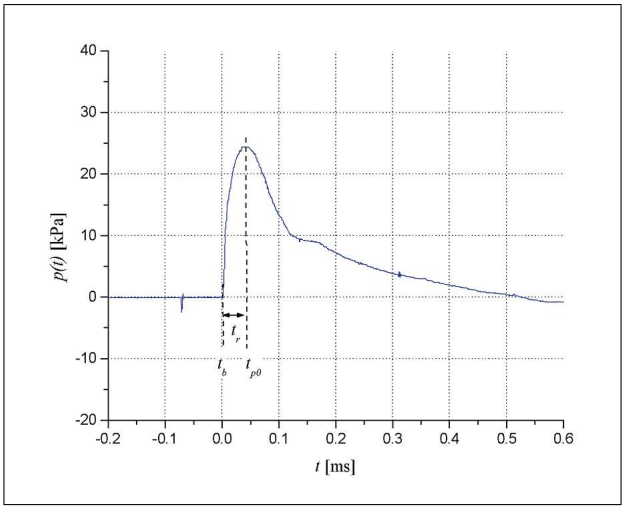


Figure 6. An example of the initial pressure pulse $p_0(t)$ normalized to a distance $r = 1$ m.

in the vicinity of the bubble volume minima. However, such information would be even irrelevant for the following discussion, where only bubbles at maximum volumes are considered. It was also verified that the thin tungsten electrodes did not induce any measurable distortion of the bubble shape.

The films have been recorded for bubbles of different sizes and different intensities of oscillations. Simultaneously, the radiated pressure waves have also been recorded. By noting the presence of the same characteristic features in all pressure records (see further, e.g. Figure 5) and verifying that in each film the bubble shape was always observed to be spherical, it was possible to conclude that in all the experiments reported here the generated bubbles can be considered spherical with good approximation. Hence, only a spherical bubble shape will be assumed in the following discussion.

As far as the radiated pressure waves are concerned, a total of 448 experimental pressure records were taken corresponding to different bubble sizes, bubble oscillation intensities, hydrophone positions $r$, gaps $d$, and so on.

An example of a typical recorded pressure wave is shown in Figure 5. As depicted in Figure 5 the recorded wave can be divided into several parts, each considered as a separate pressure pulse, denoted as $p_0(t)$, $p_1(t)$, $p_2(t)$, etc. They are defined as $p_0(t)$ being the first part spanning the time interval $(t_b, t_1)$, as $p_1(t)$ spanning the time interval $(t_1, t_2)$, and as $p_2(t)$ spanning the time interval $(t_2, t_3)$.

In underwater explosion research the pressure pulse $p_0(t)$ has a form of a shock wave [25]. However, as it will be shown later (Figure 6), in these underwater spark experiments no shock waves were radiated. As this is also the case in some other experimental works, some researchers call this part of the wave the primary pulse [1, 2, 17, 19]. However, with respect to the indexing of different events adopted in this paper, it is more convenient to refer to this pulse as the initial pulse.

The pressure pulse $p_1(t)$ will be referred to as the first bubble pulse, in agreement with underwater explosion research [25], and the pressure pulse $p_2(t)$ will be referred to as the second bubble pulse. Further pressure pulses, as $p_3(t)$, etc. are also present in the pressure records. However, as these pressure pulses are almost entirely masked by reverberation noise, they will not be considered here.

In Figure 5 the origin of the pressure scale corresponds to the acoustic pressure equal to zero: however, it must be noted that the ambient hydrostatic pressure $p_\infty$ at the sparker depth is about $1.275 \cdot 10^5$ Pa.

In each pressure record the breakdown time $t_b$ corresponds to the time when the acoustic pressure in the initial pulse $p_0(t)$ starts growing from zero value (see Figure 6, where the details of the initial pulse $p_0(t)$ are more clearly displayed). The breakdown time $t_b$ will be usually taken as the origin of the time scale. However, in some cases, as in Figure 5, the origin of the time scale is coincident with the time when the trigger pulse is sent off (time $t_0$) and the recording by the A/D board is started. The times when the pressure pulses attain their peak values are then denoted as $t_{p0}$, $t_{p1}$, and $t_{p2}$. The times when the radiated pressure attains the trough values are denoted as $t_1$, $t_2$ and $t_3$ (as mentioned above the trough pressures correspond to maximum bubble volumes). The time intervals corresponding to different bubble oscillation phases are called respectively: a) the first, second, and third bubble growth times, $T_{g1}$, $T_{g2}$ and $T_{g3}$; b) the first and second compression times $T_{c1}$ and $T_{c2}$; c) the first and second oscillation periods $T_{o1}$ and $T_{o2}$.

As it is extremely difficult to determine with adequate precision the times $t_1$, $t_2$ and $t_3$ in the experiments, since both the bubble volume and the radiated pressure vary very little in the time intervals centered on $t_1$, $t_2$ and $t_3$, it is therefore assumed that $T_{g1} = T_{c1} = T_{o1}/2$, and $T_{g2} = T_{c2} = T_{o2}/2$. From Figure 5 it then follows that $T_{o1} = t_{p1} - t_b$, $T_{o2} = t_{p2} - t_{p1}$, $T_{o1} = T_{g1} + T_{c1}$, $T_{o2} = T_{g2} + T_{c2}$, and finally $t_1 = t_b + T_{g1}$, $t_2 = t_b + T_{o1} + T_{g2}$, and $t_3 = t_b + T_{o1} + T_{o2} + T_{g3}$.

## 5. Analysis of the earliest stages

After the time $t_a$ when the capacitor is connected to the discharge electrodes, two time intervals can be considered: a pre-breakdown interval $(t_a, t_b)$, and an after-breakdown interval $(t_b, \infty)$. In the pre-breakdown interval leaders are formed in the liquid between the electrodes and a certain part of the energy $E_c$ is dissipated in the circuit [12, 21].

The dissipated energy is directly proportional to the breakdown time $t_b$. Thus the energy $E_b$ available at time $t_b$ can be lower than $E_c$ [12, 21], and will vary from one discharge to another randomly. No attempt has been done to determine $E_b$ in these experiments and it will be assumed that $E_b = E_c$. It is expected, however, that the error introduced by this approximation might be acceptable.

Breakdown of the liquid is associated with the formation of a highly conductive discharge channel between the two electrodes. As it was already mentioned, the resistance of this channel, $R_d$, is time dependent and can attain different values in different experiments even using the same experimental arrangement. Thus the Joule heat released in the channel, $E_d$, and the efficiency $\eta_d$, will also vary randomly.

The released heat will cause the pressure and temperature of the plasma and vapor in the channel to increase violently. The growth of pressure in the channel will be accompanied by a pressure increase in the surrounding liquid and this pressure change will propagate outwards in the liquid in the form of the initial pressure pulse $p_0(t)$. As this pressure wave is linked to the pressure in the channel, its form can be used to assess some of the physical processes taking place in the channel. An example of the measured initial pressure pulse $p_0(t)$ is shown in Figure 6.

The form of the initial pulse $p_0(t)$ can be interpreted in the following way. After breakdown, the pressure in the channel grows violently, and this pressure increase sets the channel boundaries into an outward motion, so that a growing bubble is formed in place of the channel. As the volume of the bubble grows, the pressure at the bubble wall keeps decreasing. Thus there are two influences acting against each other: continuously supplied heat (with time variable intensity), which tends to increase the pressure in the channel, and continuously enlarging bubble volume, which tends to decrease the pressure. At the beginning, the increase in pressure due to supplied heat will dominate. However, at a time $t_r$, which will be referred to as the rise time of the initial pressure pulse (see Figure 6), the decrease in pressure due to the bubble volume growth starts to dominate, even if heat continues to be further released in the channel, though at a lower rate.

The rise time $t_r$ seems to be a suitable parameter which can be easily determined experimentally for characterizing the initial conditions in the channel. In section 7 it will be investigated how these initial conditions, represented by the value of $t_r$, influence the properties of the generated bubble.

As it can be seen in Figure 3b, the instantaneous power $P_d(t)$ grows violently from zero to a maximum value and then it starts decreasing. In section 3 the time, when the instantaneous power $P_d(t)$ attains the maximum, was denoted as $t_{iM}$. It is now useful to examine a relation between $t_r$ and $t_{iM}$.

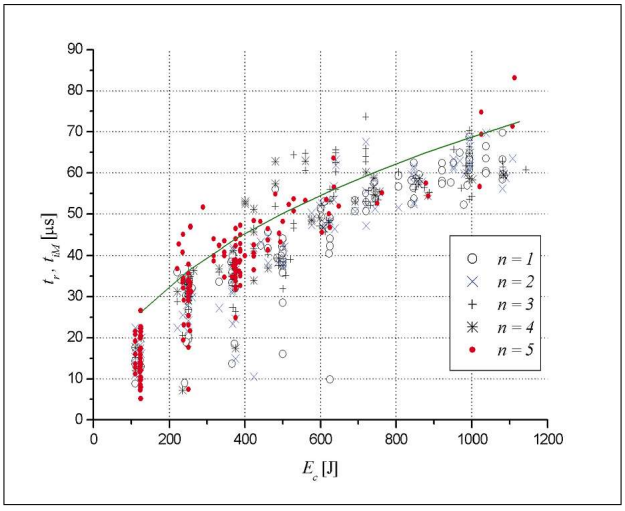


Figure 7. Variation of the rise time $t_r$ with energy $E_c$. Index $n$ is for the reversed order of discharges in a series. The solid curve corresponds to the variation of the theoretically determined time $t_{iM}$ with energy $E_c$.

The experimentally determined variation of $t_r$ versus $E_c$ is shown in Figure 7. It can be seen that $t_r$ grows with $E_c$. Also shown in Figure 7 is the variation of $t_{iM}$ versus $E_c$. The values of $t_{iM}$ have been determined from the theoretical relation (3) using the values of $L = 7.66\,\mu\text{H}$, $R = 0.065\,\Omega$ and $C = 40, \ldots, 360\,\mu\text{F}$. One can see that the time $t_{iM}$ is almost the same (or slightly larger) as $t_r$ and it can be expected that this agreement between $t_r$and $t_{iM}$ will be retained even if $t_{iM}$ could be determined experimentally.

Thus the following conclusion can be drawn. As the time $t_{iM}$ is a measure of the rate of the growth of the instantaneous power $P_d(t)$ delivered into the channel, so is also $t_r$ a measure of this rate. In other words, the shorter $t_r$ is, the faster $P_d(t)$ grows to its maximum value.

## 6. Efficiency of energy conversion

In this section the interest will be to determine experimentally the efficiencies of energy conversion in the spark discharges. The energies used to compute the efficiencies will be determined at three significant times. The first significant time, $t_0$, corresponds to the moment immediately before connecting the charged capacitor to the discharge electrodes. The second significant time, $t_1$, corresponds to the moment when the bubble attains the first maximum volume, and the third significant time, $t_2$, corresponds to the moment when the bubble attains the second maximum volume. In the following discussion, the interest will be restricted to the energies that can be directly determined from the experimental arrangement and from the measured pressure records.

The first energy that can be determined is the electrical energy available at the capacitor at the instant $t_0$. This energy is given by equation (1) and has been denoted as $E_c$. Further on the acoustic energy carried away by the pressure wave radiated by the oscillating bubble can be determined. When computing this energy a spherical pressure wave $p(t)$ will be assumed to be propagating in a liquid of density $\rho_\infty$ (for water $\rho_\infty = 10^3\,\mathrm{kg/m^3}$) with speed of sound $c_\infty$ (for water $c_\infty$ was taken to be 1480 m/s), and measured at a distance $r$ from the bubble center. Then the acoustic energy carried away by the initial pulse $p_0(t)$ is

$$E_{ap0} = 4\pi r^2 \frac{1}{\rho_\infty c_\infty} \int_{t_b}^{t_1} p^2(t)\,\mathrm{d}t, \tag{9}$$

and the acoustic energy carried away by the first bubble pulse $p_1(t)$ is

$$E_{ap1} = 4\pi r^2 \frac{1}{\rho_\infty c_\infty} \int_{t_1}^{t_2} p^2(t)\,\mathrm{d}t. \tag{10}$$

From the pressure records one can also easily determine the first and second period of bubble oscillation $T_{o1}$ and $T_{o2}$, respectively. Assuming that the spherical bubble oscillates with sufficient intensity, then the value of the dimensionless time of the bubble compression is $T_{zc1} = 0.92$ [26]. The dimensionless time $T_{zc1}$ is defined as [26]

$$T_{zc1} = \frac{T_{c1}}{R_{M1}\sqrt{\rho_\infty / p_\infty}}. \tag{11}$$

Hence the first maximum bubble radius $R_{M1}$ can be determined from $T_{o1}$ as ($T_{c1} \approx T_{o1}/2$)

$$R_{M1} = \frac{T_{o1}}{1.84\sqrt{\rho_\infty / p_\infty}}. \tag{12}$$

The knowledge of $R_{M1}$ makes it possible to estimate the first maximum bubble potential energy at $t_1$,

$$E_{\mathrm{pot1}} = \frac{4}{3}\pi\, p_\infty\, R_{M1}^3. \tag{13}$$

In the same way the second bubble maximum radius $R_{M2}$ can be determined

$$R_{M2} = \frac{T_{o2}}{1.84\sqrt{\rho_\infty / p_\infty}}, \tag{14}$$

and the corresponding potential energy at $t_2$ is

$$E_{\mathrm{pot2}} = \frac{4}{3}\pi\, p_\infty\, R_{M2}^3. \tag{15}$$

Hence, to summarize, the considered energies are as follows:

at $t_0$: $E_c$,
at $t_1$: $E_{ap0}$, $E_{\mathrm{pot1}}$,
at $t_2$: $E_{ap1}$, $E_{\mathrm{pot2}}$.

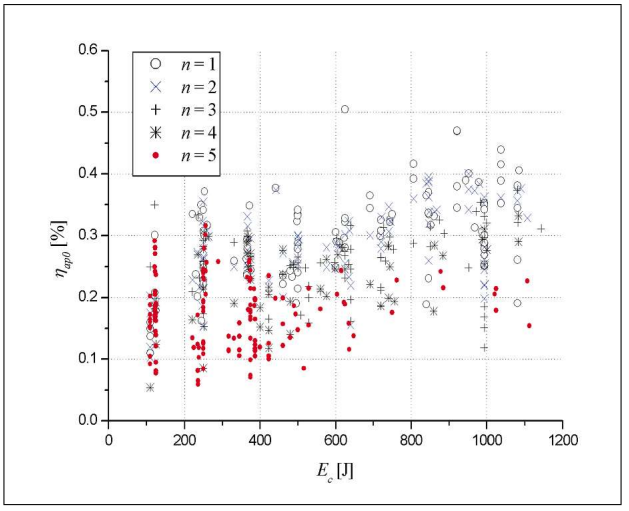


Figure 8. Variation of the efficiency $\eta_{ap0}$ with energy $E_c$. Index $n$ is for the reversed order of discharges in a series.

As one is often interested in using underwater sparks as sources of high-intensity acoustic pulses, then it may be interesting to calculate the efficiencies with which the energy available at $t_0$ (i.e. $E_c$) is converted into the acoustic energies $E_{ap0}$ and $E_{ap1}$, i.e.

$$\eta_{ap0} = \frac{E_{ap0}}{E_c} 100, \quad [\%], \tag{16}$$

$$\eta_{ap1} = \frac{E_{ap1}}{E_c} 100, \quad [\%], \tag{17}$$

and to calculate the efficiencies with which the bubble attains the potential energies $E_{\mathrm{pot1}}$ and $E_{\mathrm{pot2}}$, i.e.

$$\eta_{\mathrm{pot1}} = \frac{E_{\mathrm{pot1}}}{E_c} 100, \quad [\%], \tag{18}$$

$$\eta_{\mathrm{pot2}} = \frac{E_{\mathrm{pot2}}}{E_c} 100, \quad [\%]. \tag{19}$$

The mentioned efficiencies calculated from experimental records are shown in Figures 8–11. In these graphs, the parameter is the index $n$ of the individual discharge record counted from the end of each series. It can be seen that the data points corresponding to $n = 1$ (the largest $R_{d\,\mathrm{ef}}$) have a tendency to occur at the highest values of efficiencies. However, no distinctive separation of the values corresponding to different $n$ can be seen.

Efficiencies displayed in Figures 8–11 show a rather large scatter and possibly even some underlying trends. At present time there is no clear physical explanation for the large scatter and possible trends. An exact measurement of $R_d(t)$ might throw some light on this problem, although it would not probably clarify all questions which remain not understood. Another question regarding Figures 8–11 concerns the minimum size of the data set. Since in spark discharges some randomness is always present, one may ask how large must the data set be, to be statistically representative. Our data were taken from a set of 448 records, obtained using 9 different capacities. The

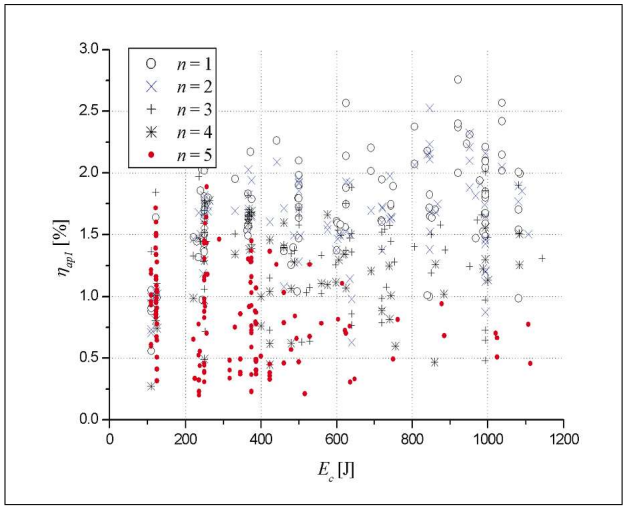


Figure 9. Variation of the efficiency $\eta_{ap1}$ with energy $E_c$. Index $n$ is for the reversed order of discharges in a series.

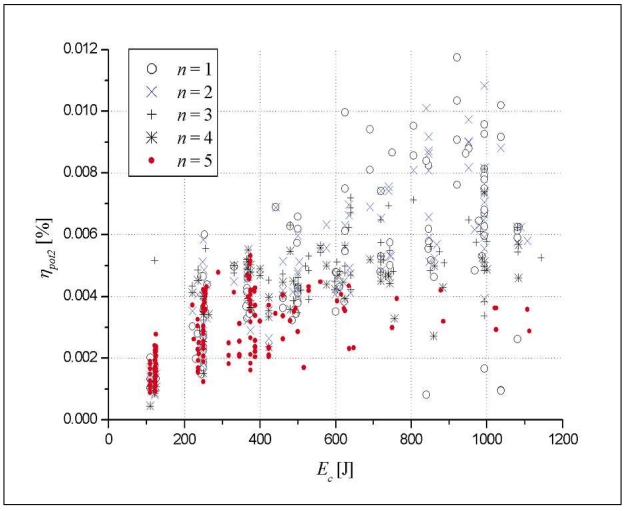


Figure 11. Variation of the efficiency $\eta_{\text{pot2}}$ with energy $E_c$. Index $n$ is for the reversed order of discharges in a series.

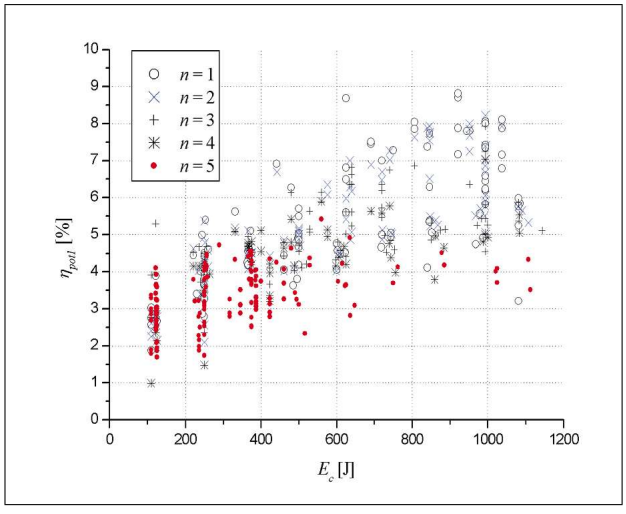


Figure 10. Variation of the efficiency $\eta_{\text{pot1}}$ with energy $E_c$. Index $n$ is for the reversed order of discharges in a series.

data corresponding to each capacity were grouped into 5 classes according to the value of index $n$, and also grouped into 5 classes according to the value of voltage $V$. Thus one final class consists, on average, of only 2 elements and this is certainly insufficient. It is therefore quite possible that as more data will become available, the trends would simply disappear, or, on the other hand, would become even more pronounced.

As can be seen from Figures 8–11, in the time interval $(t_0, t_1)$, a much larger part of energy $E_c$ is converted into the potential energy $E_{\text{pot1}}$ than into the acoustic energy $E_{ap0}$ ($E_{\text{pot1}} \approx 20E_{ap0}$) and in the time interval $(t_1, t_2)$, a much larger part of the energy $E_c$ is converted into the acoustic energy $E_{ap1}$ than into the potential energy $E_{\text{pot2}}$ ($E_{ap1} \approx 250E_{\text{pot2}}$). Thus $E_{ap0}$ and $E_{\text{pot2}}2$ play only a minor role in determining the efficiency of energy conversion at characteristic times $t_1$ and $t_2$.

Further, it can be seen that only from 2% to 8% of the energy available at the instant $t_0$ is converted into potential energy $E_{\text{pot1}}$ at the time $t_1$, and only about 30% of the potential energy $E_{\text{pot1}}$ available at the time $t_1$ is radiated away from the bubble as acoustic energy $E_{ap1}$ during the time interval $(t_1, t_2)$. This means that in the time interval $(t_0, t_1)$ about 92% to 98% of the energy $E_c$ is converted into other forms of energy than $E_{\text{pot1}}$ and in the time interval $(t_1, t_2)$ about 70% of the energy $E_{\text{pot1}}$ is converted into energies which still need to be accounted for.

A brief discussion now follows on the energies, which are not taken into account here. It can be expected that by far the largest part of energy at time $t_1$ can be attributed to Joule heat released in resistors $R_i$, $R_a$ and $R_c$. Another significant part of energy is lost as optical radiation: however, no direct experimental results can be found in literature in this respect. In some works [15, 20] theoretical computations of several energies associated with spark discharges are given. However, it seems that in these computations some parameters can be set rather arbitrarily to obtain the desired result.

Using the values of efficiency mentioned above and the values of $R_{d\,\text{mean1}}$ and $R_{\text{mean1}}$ determined in section 3, a rough estimate can be obtained of the energies not taken into account here at the time interval $(t_0, t_1)$. By putting $R_{d\,\text{ef}} = R_{d\,\text{mean1}}$ and $R_{\text{ef}} = R_{\text{mean1}}$, then from equation (6) the efficiency of energy $E_c$ delivery into the discharge channel can be computed to be approximately 19%. Thus 81% of $E_c$ is converted into Joule heat in the connecting cables and air-gap switch. From the 19% of $E_c$ delivered into the discharge channel, about 2–8% can be subtracted as being converted into $E_{\text{pot1}}$. Thus approximately 11–17% of $E_c$ are converted into optical radiation and other processes associated with vapor ionization in the discharge channel.

As far as the interval $(t_1, t_2)$ is concerned, the existence of unaccounted for losses accompanying bubble oscillations has already been reported in connection with underwater explosions [27]. Further analysis of experimental data and discussion of these losses can be found elsewhere

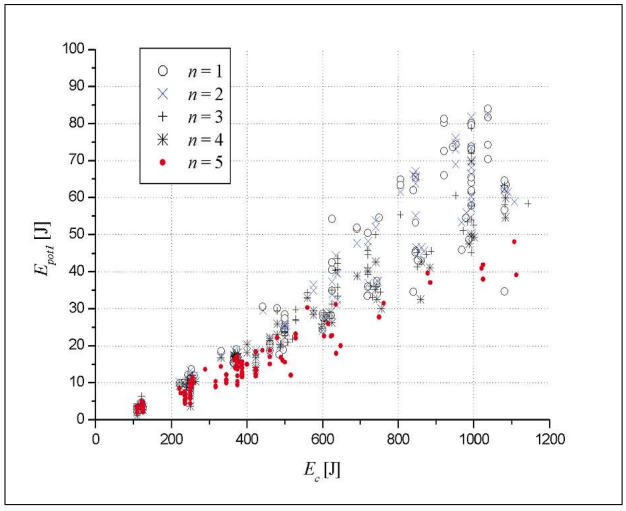


Figure 12. Variation of the energy $E_{\mathrm{pot1}}$ with energy $E_c$. Index $n$ is for the reversed order of discharges in a series.

[26]. However, it is remarked that no satisfactory explanation for these losses has been given so far, although they represent as much as 70% of energy $R_{\mathrm{pot1}}$ available at time $t_1$.

Finally, the present results can be compared with data published in other works. For example, Naugolnych and Roy [12] give several values of $\eta_{\mathrm{pot1}}$ (see Table 2.2 in [12]) ranging from about 2.3% to 7.2%. These values are in good agreement with the present data given in Figure 10. The variation of $E_{ap0}$ with $E_c$ has been determined by Cook *et al.* [16] (see Figure 16 in [16]). From these data it can be estimated that $\eta_{ap0}$ was about 3% in the respective experiments. This value is higher by a factor of about 10 compared with the present data given in Figure 8. Unfortunately, the experimental data published in the reference [16] were reproduced from a report which is not available to the present authors, so it is difficult to discuss the reason for this difference. It can only be suspected that the discharge circuit parameters were probably much different from the ones reported here. The experiments were also done at sea under much higher ambient pressures. Last but not least, seawater salinity can change the evolution of a spark discharge considerably. And all these factors could influence the value of $\eta_{ap0}$.

## 7. Relation between the spark discharge and generated bubble

In section 1 it has been already mentioned that an oscillating bubble generated by a spark discharge is described by its size and intensity of oscillation. The bubble size can be conveniently characterized by the first maximum radius $R_{M1}$ [23], which is directly connected with the potential energy $E_{\mathrm{pot1}}$ (cf. equation 13). As far as the intensity of bubble oscillation is concerned, it has been shown [26] that it is directly proportional to the radiated acoustic energy in the first bubble pulse $E_{ap1}$. In this section it will be investigated how these two quantities representing the bubble size and intensity of oscillations, that is $E_{\mathrm{pot1}}$ and $E_{ap1}$, are influenced by the parameters of the discharge circuit.

First it will be examined how these two energies vary with the energy available for the discharge $E_c$. The variation of $E_{\mathrm{pot1}}$ with $E_c$ is shown in Figure 12. As it can be seen, the potential energy of the bubble, $E_{\mathrm{pot1}}$, grows with $E_c$. Thus it can be concluded that to generate larger bubbles, larger energies $E_c$ are needed. This assertion will be most probably not valid generally, but rather it can be expected to hold for a given apparatus only and for a certain range of energies $E_c$.

The acoustic energy $E_{ap1}$ is converted from the potential energy $E_{\mathrm{pot1}}$ during the bubble oscillation first of all [8] and therefore it will also grow with $E_{\mathrm{pot1}}$. To eliminate this dependence on the bubble size and retain only the dependence of $E_{ap1}$ on the bubble oscillation intensity, the normalized acoustic energy $E_{zap1}$, defined as

$$E_{zap1} = E_{ap1}/E_{\mathrm{pot1}} \tag{20}$$

will be considered in the following. It is to be noted that $E_{zap1}$ is a dimensionless energy whose value is in the interval $(0, 1)$; however, for an easier comparison with other efficiencies computed in this paper $E_{zap1}$ will be also expressed in %. The dimensionless energy $E_{zap1}$ is being used here in two roles. First, it can be used as a measure of efficiency of converting the potential energy $E_{\mathrm{pot1}}$ into acoustic energy $E_{ap1}$. However, it can be also used as a measure of the bubble oscillation intensity. As shown in references [23, 26], the dimensionless energy $E_{zap1}$ grows continuously with another measure of bubble oscillation intensity, namely with the amplitude of bubble oscillations. And this second role of $E_{zap1}$, linked to the bubble oscillation intensity, is also often referred to in this paper.

The variation of $E_{zap1}$ with $E_c$ is shown in Figure 13a. Now the scatter of data is much larger than in Figure 12 and no clear dependence of $E_{zap1}$ on $E_c$ can be detected. However, two hypotheses can be suggested to explain the spreading of data points in this figure. In this respect two things can be observed. The first observation concerns the variation of the maximum value of $E_{zap1}$ with $E_c$. The second observation concerns the span between the maximum and minimum values of $E_{zap1}$ for a given $E_c$. To explain the first observation, the suggested hypothesis is that the maximum intensity of oscillation the bubble is excited to is determined by the rate of energy delivery into the discharge channel. To explain the wide range of bubble oscillation intensities a second hypothesis is that the intensity of bubble oscillations for given values of capacity $C$ and charge voltage $V$ is determined by the efficiency $\eta_d$, with which the electrical energy is converted into heat in the discharge channel.

To support the first hypothesis, the maximum values of $E_{zap1}$ will be considered, by following the upper contour of the displayed points in Figure 13a. As it can be seen, the maximum values of $E_{zap1}$ grow with $E_c$ for $E_c < 250\,\mathrm{J}$, attain a maximum for $E_c \approx 250\,\mathrm{J}$, and decrease with $E_c$ for $E_c > 250\,\mathrm{J}$. By observing the upper contour of $E_{zap1}$ values more carefully, a saw-tooth like contour appears which

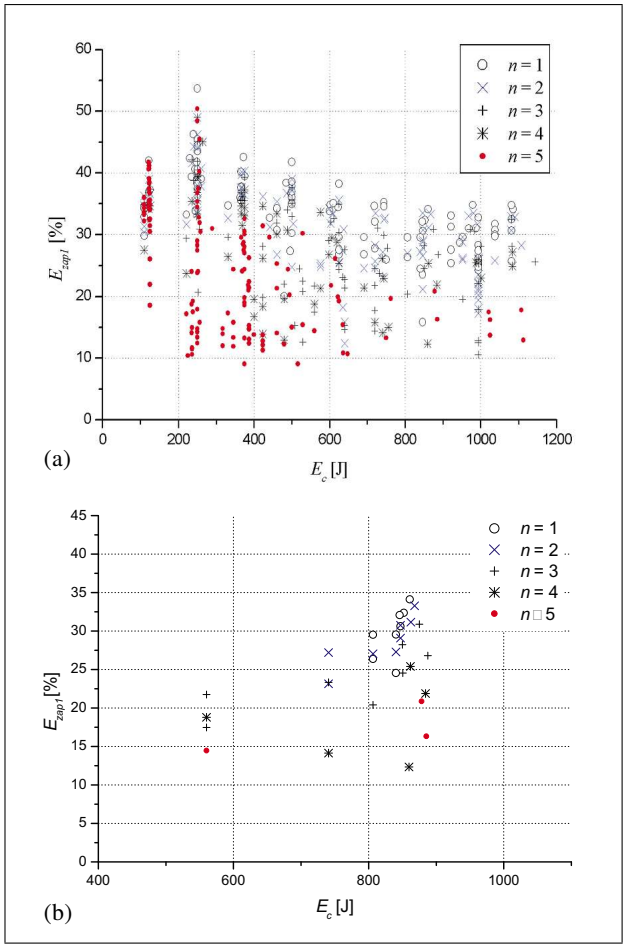


Figure 13. a. Variation of the normalized acoustic energy $E_{zap1}$ with energy $E_c$ for all values of capacitance $C$. Index $n$ is for the reversed order of discharges in a series. b. Variation of the normalized acoustic energy $E_{zap1}$ with energy $E_c$ in the case of capacitance $C = 280\,\mu$F. Index $n$ is for the reversed order of discharges in a series.

is a result of the overlapping of regions corresponding to different capacities $C$. (A similar effect could also be observed in Figure 12, with the only difference that in this case the regions are linked almost smoothly and therefore no saw-tooth-like contour is visible.) An example of one of the regions taken from Figure 13a is given in Figure 13b.

Recalling from equation (1) that for a given capacitance $C$ the energy $E_c$ is increasing with charging voltage $V$, it follows from Figure 13b that, when $E_c$ is increasing, the range of possible values of $E_{zap1}$ is also increasing. Even more, the bubbles can be excited to oscillate with the highest intensities when for a given capacitance $C$ the voltage $V$ attains its maximum value. This can be easily understood realizing that for a given $C$ and for a given efficiency $\eta_d$ a higher voltage $V$ means a larger discharge current $i(t)$ and thus also a higher possible power $P_d$ delivered into the channel.

The second fact which can be observed in Figure 13a concerns the wide range of possible values of $E_{zap1}$ (i.e., of possible intensities of bubble oscillations) for a given electric energy $E_c$. To explain this fact a second hypothesis

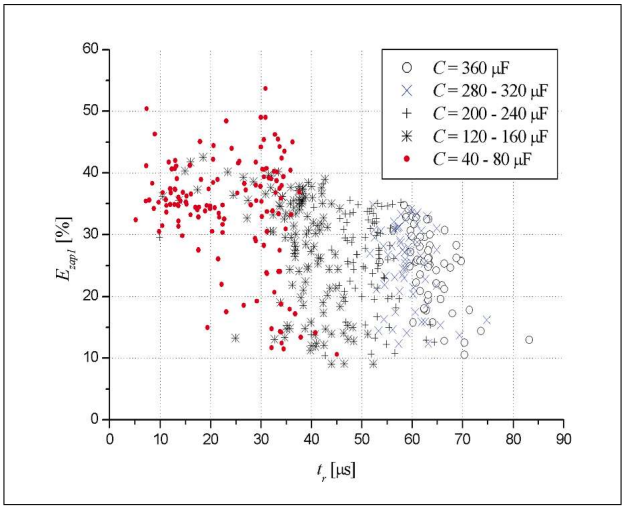


Figure 14. Variation of the normalized acoustic energy $E_{zap1}$ with the rise time of the initial pressure pulse $t_r$, for different values of capacitance $C$.

is that for given $C$ and $V$ the intensity of bubble oscillations is increasing with the efficiency $\eta_d$ of electric energy conversion into heat in the discharge channel. As it can be seen in Figure 13b, the highest values of $E_{zap1}$ (corresponding to the highest intensities of bubble oscillations) are concentrated at the upper right corner of the cluster of points and these highest values of $E_{zap1}$ correspond to $n = 1$, that is to the last successful discharges in the series, when the gap $d$ was the largest and thus also the discharge resistance $R_d$ was the largest. And according to equation (11), the large values of $R_d$ correspond to large values of $\eta_d$. On the other hand, it can be seen in Figure 13b, that the points corresponding to $n \geq 4$ are concentrated at the lower part of the cluster of points. Using a similar reasoning it follows immediately that the points corresponding to the lowest values of $E_{zap1}$ (and thus to the lowest values of bubble oscillation intensity) correspond to the lowest efficiencies $\eta_d$.

Returning to the first hypothesis concerning the rate of power delivery into the discharge channel, three parameters can be identified in the discharge circuit which varied in the present experiments: the capacitance $C$, the charging voltage $V$, and the discharge channel resistance $R_{def}$. In the following, the influence of each of these parameters shall be analyzed briefly.

First the capacitance $C$ will be considered, to verify the hypothesis that the maximum intensity of oscillation the bubble can be driven to is inversely proportional to the time $t_{iM}$ needed for the instantaneous power $P_d(t)$ to reach its maximum.

As shown in Figure 7, there is a correlation between the theoretically determined time $t_{iM}$ and the experimentally determined time $t_r$. Thus, to verify the above hypothesis the variation of $E_{zap1}$ with $t_r$ can be examined. This variation is shown in Figure 14.

By analyzing equation (3) it can be seen that the time $t_{iM}$ varies both with $C$ and $R$. However, numerical computations based on equation (3) have shown that the varia-

tion of $t_{iM}$ with $R$ is much smaller than the variation of $t_{iM}$ with $C$. This can also be verified in Figure 14, where the parameter is the capacitance $C$. By a closer examination of Figure 14 it can be seen that the values of $E_{zap1}$ corresponding to a given $C$ are enclosed, roughly, by a box having a rectangular form. This shows that within each rectangle the normalized energy $E_{zap1}$ does not vary with $t_r$, or, in other words, $t_r$ is constant for a given $C$. Thus, the experimentally determined influence of $R$ on $t_r$ is negligible and the drop in maximum values of $E_{zap1}$ is solely due to an increase in the value of $t_r$ caused by an increase in the value of $C$.

As it can be seen in Figure 14, the highest values of $E_{zap1}$ correspond to $C = 80\,\mu F$. A clear explanation for this local maximum was not found at present time. It is only remarked that a distinct behavior of the experimental values corresponding to this capacitance (and also to $C = 120–160\,\mu F$) can be seen in many graphs.

It should also be remarked that both $E_{pot1}$ and $E_{zap1}$ grow with decreasing $n$ (that is, with increasing $R_{def}$). However, the influence of capacity $C$ is reversed in these cases. Whereas $E_{pot1}$ grows with $C$, and the values of $E_{pot1}$ are relatively well separated for different $C$, the values of $E_{zap1}$ overlap heavily for different $C$ and decrease with increasing $C$.

The final remark concerns the growth of the maximum values of $E_{zap1}$ (and thus also of the maximum bubble oscillation intensities) with voltage $V$. A closer look at Figure 13b reveals that at a certain value of $V$ (approximately at $V = 2.5\,kV$) the dimensionless energy $E_{zap1}$ attains its highest values. Above this voltage the maximum values of $E_{zap1}$ are decreasing. This effect has been observed for all condenser capacities $C$. Again, there seems to be no explanation at present time for this behavior, which is mentioned here just for the sake of completeness.

## 8. Conclusions

Underwater spark discharges and associated bubble oscillations represent complex dynamic nonlinear phenomena accompanied, among others, by emission of intensive pressure waves. In this work, by using high-energy low-voltage spark discharges, a wide range of bubble sizes and intensities of their oscillation was generated. Such a wide range (scatter) of values might be probably considered to be an inconvenience in applications exploiting spark discharges as impulsive acoustic sources, because in these applications a good repeatability of the radiated waves is required. However, in studying bubble dynamics this scatter in both bubble sizes and intensities of oscillation seems to be very valuable and it is intended to exploit this in further works.

In this paper, by analyzing a relatively large set of recorded pressure waves emitted by spark discharges and associated oscillating bubbles, it was tried to gain a better insight into these phenomena. In particular, the main interest was in determining the efficiencies of conversion of the available electrical energy into potential energy of the generated bubbles and into acoustic energy radiated during oscillations of these bubbles. When determining the acoustic energy, the existence of large unaccounted for energy losses associated with bubble oscillations, was confirmed. By analyzing the spark discharge circuit and the early stages of the discharges it was also tried to clarify the relations between the discharge circuit parameters, the potential energy of the generated bubbles and the radiated acoustic energy. It was shown that, within the present experimental conditions, the potential energy of the bubbles grows with the energy available for the discharge. However, the relation between the discharge circuit parameters and the radiated acoustic energy showed to be more complex. It was verified that, within certain limits, the intensity of bubble oscillations and thus also the relative value of acoustic energy (expressed as the ratio of radiated acoustic energy to bubble potential energy) is directly proportional to the rate of power delivery into the discharge channel. However, with respect to the intensity of bubble oscillations, an even more critical point seems to be the efficiency of available electrical energy deposition into the discharge channel, which is given as the ratio of the effective discharge channel resistance to the total discharge circuit resistance.

Some other supplementary observations have also been mentioned in the paper. However, not all questions concerning these complex phenomena have been clarified. For example, it can be expected that there is some limit to increasing the bubble intensity of oscillation by increasing the rate of power delivery into the discharge channel. Most probably, when increasing the rate of power delivery, an increasingly larger part of the delivered energy will be radiated in the form of both acoustic energy associated with the initial pressure pulse and optical energy. Hence, the increase of bubble intensity of oscillation will eventually reach some limit. However, to verify this hypothesis, a different experimental arrangement compared to that used here will be needed.

### Acknowledgement

This work has been partly (K.V.) supported by the Ministry of Education of the Czech Republic as research project MSM 467 478 8501.

### References

[1] G. B. Cannelli, E. D'Ottavi, A. Prosperetti: Bubble activity induced by high-power marine sources. Oceans '90, Washington, D.C., September 24–26, 1990, 533–537.

[2] G. B. Cannelli, E. D'Ottavi: Physical phenomena involved in sea-water plasma based sound source. European conference on underwater acoustics, Luxembourg, September 14–18, 1992, 635–638.

[3] L. H. Fry, J. P. Adair, R. Williams: Long life sparker for pulse powered underwater acoustic transducer. 12th IEEE International Pulsed Power Conference, Monterey, CA, USA, June 27–30, 1999, Vol. 2, 781–784.

[4] M. Bourlion, P. Dancer, F. Lacoste, J.-L. Mestas, D. Cathignol: Design and characterization of a shock wave generator using canalized electrical discharge: Application to lithotripsy. Rev. Sci. Instrum. **65** (1994) 2356–2363.

[5] M. R. Bailey, D. T. Blackstock, R. O. Cleveland, L. A. Crum: Comparison of electrohydraulic lithotripters with rigid and pressure-release ellipsoidal reflectors. I. Acoustic fields. J. Acoust. Soc. Am. **104** (1998) 2517–2524.

[6] P. Šunka, V. Babický, M. Člupek, J. Beneš, P. Poučková: Localized damage of tissues induced by focused shock waves. IEEE Transactions on Plasma Science **32** (2004) 1609–1613.

[7] R. H. Mellen: An experimental study of the collapse of a spherical cavity in water. J. Acoust. Soc. Am. **28** (1956) 447–454.

[8] K. Vokurka: Evaluation of data from experiments with spark and laser generated bubbles. Czech. J. Phys. **B 38** (1988) 35–46.

[9] J. R. Krieger, G. L. Chahine: Acoustic signals of underwater explosions near surfaces. J. Acoust. Soc. Am. **118** (2005) 2961–2974.

[10] E. A. Martin: Experimental investigation of high-energy density, high-pressure arc plasma. J. Appl. Phys. **31** (1960) 255–267.

[11] D. D. Caulfield: Predicting sonic pulse shapes of underwater spark discharges. Deep-Sea Res. **9** (1962) 339–348.

[12] K. A. Naugolnych, N. A. Roy: Spark discharges in water (in Russian). Nauka, Moscow, 1971.

[13] R. Kattan, A. Denat, O. Lesaint: Generation, growth, and collapse of vapor bubbles in hydrocarbon liquids under a high divergent electric field. J. Appl. Phys. **66** (1989) 4062–4066.

[14] A. H. Olson, S. P. Sutton: The physical mechanisms leading to electrical breakdown in underwater arc sound sources. J. Acoust. Soc. Am. **94** (1993) 2226–2231.

[15] R. M. Roberts, J. A. Cook, R. L. Rogers, A. M. Gleeson, T. A. Griffy: The energy partition of underwater sparks. J. Acoust. Soc. Am. **99** (1996) 3465–3475.

[16] J. A. Cook, A. M. Gleeson, R. M. Roberts, R. L. Rogers: A spark-generated bubble model with semi-empirical mass transport. J. Acoust. Soc. Am. **101** (1997) 1908–1920.

[17] S. Buogo, G. B. Cannelli, E. D'Ottavi, L. Pitolli, G. Pontuale: Bubble influence on the behaviour of sea-water plasma-based sound sources. Acustica united with Acta Acustica **84** (1998) 1025–1030.

[18] F. Jomni, F. Aitken, A. Denat: Experimental investigation of transient pressure waves produced in dielectric liquids. J. Acoust. Soc. Am. **107** (2000) 1203–1211.

[19] S. Buogo, G. B. Cannelli: Implosion of an underwater spark-generated bubble and acoustic energy evaluation using the Rayleigh model. J. Acoust. Soc. Am. **111** (2002) 2594–2600.

[20] X. Lu, Y. Pan, K. Liu, M. Liu: Spark model of pulsed discharge in water. J. Appl. Phys. **91** (2002) 24–31.

[21] A. Grinenko, A. Sayapin, V. T. Gurovich, S. Efimov, J. Felsteiner, Y. E. Krasik: Underwater electrical explosion of a Cu wire. J. Appl. Phys. **97** (2005) 1–6.

[22] J. W. Mackersie, I. V. Timoshkin, S. J. MacGregor: Generation of high-power ultrasound by spark discharges in water. IEEE Transactions on Plasma Science **33** (2005) 1715–1724.

[23] K. Vokurka: Amplitudes of free bubble oscillations in liquids. J. Sound Vib. **141** (1990) 259–275.

[24] S. Buogo, G. B. Cannelli, K. Vokurka: Observation of spherical growth and collapse of a spark bubble in water. Seventh European Conference on Underwater Acoustics, ECUA 2004, Delft, The Netherlands, July 5–8, 2004, Proceedings: TNO Physics and Electronics Laboratory, The Hague, The Netherlands, 2004, D. G. Simons, ed.

[25] R. H. Cole: Underwater explosions. Princeton University Press, Princeton, 1948.

[26] K. Vokurka: A method for evaluating experimental data in bubble dynamics studies. Czech. J. Phys. **B 36** (1986) 600–615.

[27] A. B. Arons, D. R. Yennie: Energy partition in underwater explosion phenomena. Reviews of Modern Physics **20** (1948) 519–536.